JOURNAL OF PROPULSION AND POWER
Vol. 12, No. 4, July–August 1996

Experimental Investigation of a Nonsteady Flow Thrust Augmenter

Sameh M. Amin* and Charles A. Garris Jr.†
George Washington University, Washington, D.C. 20052

A comparative experimental study of the flowfields within a nonsteady flow ejector and a steady-flow ejector with similar geometry was conducted under static conditions in open air. The nonsteady flow ejector was of the rotating primary type where the primary was integral with the shroud. The goals of the study were to divulge why previous experimental investigations failed to realize the levels of performance predicted by theory, what are the strengths and weaknesses of theoretical models, and how future designs might be improved. The experiments consisted of traversing the flowfields of both ejectors with suitable probes to determine axial, tangential, and radial velocity components, and local stagnation pressure. Flow visualization experiments were also performed. The results demonstrated the short pressure exchange phase assumed by the theory. Also shown are the stabilizing effects of the rotating primaries in both lateral mixing and in diffuser performance in comparison with the steady flow ejector. An energetically more efficient nonsteady flow induction process is indicated by the stagnation pressure field. Design considerations for rotating primary ejectors are discussed and the possibility of shorter ejectors is explored.

Nomenclature

A = cross-sectional area of flow passage
f = turbulent and viscous shear forces
h^0 = specific stagnation enthalpy
m = mass flow rate
p = local static pressure
s = specific entropy
T = local static temperature
t = time
$\boldsymbol{u}$ = local fluid velocity vector
α = rotor nozzle coning angle
β = rotor nozzle spin angle
ρ = local fluid density
ϕ = thrust augmentation ratio

Subscripts
atm = atmospheric conditions
e = exit conditions
p = primary section of ejector flow
s = secondary section of ejector flow

Introduction

EJECTOR technology has long been known as a means for augmenting thrust or mass flow in a variety of propulsion applications. All ejectors enable a secondary flow to be energized by the work of a primary flow. With a conventional steady flow ejector, this work is performed through turbulent entrainment in the shear layer separating primary and secondary flows. A schematic diagram of a conventional steady-flow ejector is shown in Fig. 1a.

Another mechanism by which the primary flow can do work on the secondary is one that exists only in nonsteady flow: the work of interface pressure forces. With this mechanism, a moving pressure interface physically pushes the secondary flow. Since stationary pressure forces can do no work, this mode of energy transfer exists only in nonsteady flow. Unlike the former, this mechanism is a nondissipative and reversible process.

The roles of these two mechanisms can readily be demonstrated mathematically through the energy equation:

$$\frac{Dh^0}{Dt} = \frac{1}{\rho}\frac{\partial p}{\partial t} + T\frac{Ds}{Dt} + \frac{1}{\rho}\boldsymbol{u}\cdot f \tag{1}$$

If one imagines a fluid particle entering the ejector through the primary with h^0, Eq. (1) delineates the physical mechanisms through which this particle can exchange energy with the secondary flow. (One can similarly interpret the equation in terms of a particle entering the ejector through the secondary.) The first term on the right represents the reversible work of interface pressure forces utilized in nonsteady flow ejectors. The second term on the right represents the effects of thermal transport to or from the secondary. The third term represents the irreversible work of viscous and turbulent shear stresses and is the mechanism normally exploited in conventional steady-flow ejectors.

The benefits derived by ejectors designed to utilize the nonsteady effect were known since World War II when unexpected levels of performance were seen in the German V-1 buzz-bomb missiles. For ejector applications, this phenomenon was explored in detail by Lockwood and Patterson,[1] who used pulsating jets to produce the nonsteadiness. However, it was learned that although the pulsations can produce a dramatic improvement in thrust augmentation, the energy required to generate the pulses tends to offset the advantages. Foa[2] invented a nonsteady flow ejector that is capable of yielding the advantages of nonsteady flow, being nonsteady in the laboratory frame of reference, yet is a steady-flow in the rotor frame of reference. This type of flow was called a crypto-steady flow and the most practical configuration embodying this concept is the rotary–jet ejector. The rotary–jet ejector, utilizing the benefits of nonsteady flow, has been analyzed theoretically by Foa,[2,3] Hohenemser and Porter,[4] and Costopoulos,[5] who developed useful theoretical models.

Presented as Paper 95-2802 at the AIAA/ASME/SAE/ASEE 31st Joint Propulsion Conference and Exhibit, San Diego, CA, July 10–12, 1995; received Aug. 13, 1995; revision received Feb. 17, 1996; accepted for publication March 1, 1996.

*Research Assistant, Department of Civil, Mechanical, and Environmental Engineering.

†Professor of Engineering, Department of Civil, Mechanical, and Environmental Engineering. Member AIAA.

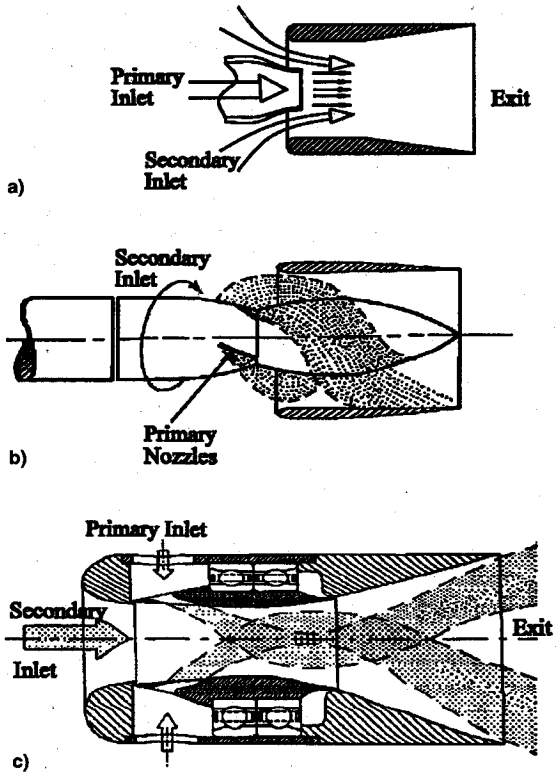

Fig. 1 Types of ejectors: a) steady-flow, b) rotary–jet, and c) hubless rotary–jet ejectors.

Among the important findings of these theoretical analyses were the following:

1) Thrust augmentations far in excess of those theoretically possible with conventional steady-flow ejectors were predicted. These thrust augmentations increased with the spin-angle (or peripheral speed) of the rotor.

2) Foa[3] showed that any form of mechanical energy dissipation can severely reduce thrust augmentation. Mechanical energy is typically dissipated through turbulent mixing or through shocks, but is conserved in interactions involving the work of interface pressure forces.

3) For low spin angles, Costopoulos[5] showed that the work of turbulent shear stresses and the work of interface pressure forces combine to augment thrust. However, for large spin angles, the dominant effect is the work of interface pressure forces.

4) Hohenemser and Porter[4] hypothesized that the work of interface pressure forces occurs very rapidly during a deflection phase, whereby the primary and secondary mutually deflect to form a common orientation in the rotor frame of reference. For this reason, Hohenemser noted that a nonsteady flow ejector can be very short in length compared to a conventional ejector.

5) Hohenemser and Porter[4] showed that turbulent entrainment during the deflection phase can have deleterious effects.

6) Foa[3] showed that when the spin angle is large, the thrust augmentation of a rotary jet ejector increases with the ratio of primary-to-secondary static temperature. This behavior is counter to the behavior of conventional ejectors where a hot primary causes a deterioration in performance. This is particularly important for aircraft applications where the primary is provided by the engine exhaust or through taps from the engine compressor. Experiments by Hohenemser and McBrayer,[8] and Porter[10] confirmed this effect.

While numerous experimental investigations by Foa and Garris,[6] Sladky,[9] Porter,[10] Hohenemser,[7] and others confirmed the beneficial effects of the rotary–jet ejector, in all cases the level of performance fell short of the theoretical predictions by a wide margin. It is possible that the theoretical models did not capture some of the complex interactions existing in the actual ejector. On the other hand, it is possible, given the large number of design variables, that none of these ejectors approached the optimal level of performance. An important goal of this study is to explore the merits and validity of these explanations.

Rotary–Jet Ejector

Figure 1b is a schematic diagram of a rotary–jet thrust-augmenting ejector. Several canted nozzles oriented at a meridional angle known as the spin-angle β, and with an angle relative to the axis of rotation known as the coning angle α, are situated in the rotor. The rotor is self-driven by the exiting jets and is free spinning, ideally experiencing negligible-bearing torque. The rotary–jet, first analyzed by Foa,[2] produces flow induction via pseudoblades of fluid that form pockets that trap the secondary flow and drives it through the ejector by virtue of the interface pressure forces, or pressure exchange. This mechanism is analogous to that of a screw-pump whereby fluid motion is induced by coercion through helical interstitial passages. A review of the prior work and the performance characteristics is presented by Garris et al.[12]

Observation of Fig. 1b clearly suggests the complexity of the crypto-steady flowfield. Since the rotor is free spinning with an assumed negligible-bearing torque, and since the initial angular momentum of both primary and secondary flowfield is zero, conservation of angular momentum requires that the net angular momentum at discharge must be zero. This implies that in the laboratory frame of reference, the primary flow emerges from the pressure exchange process counter-rotating with respect to the rotor, while the secondary emerges corotating. Further complicating the flowfield is the unavoidable presence of turbulent mixing.

Hubless Rotary–Jet

Recently, a new concept in rotary–jet design that was suggested by Cordier,[11] known as the hubless rotary–jet, was investigated by Garris et al.[12] A schematic diagram of this configuration is shown in Fig. 1c. It may be seen that the nozzles are placed on the inner surface of the shroud on a rotating cylindrical section. In the present model, the nozzle plane closely corresponds to the throat of the shroud and the nozzles are of circular cross section. As with previous rotary–jet configurations, air is fed into a plenum and directed to the nozzles. The rotor is free-spinning and self-propelled by the jets that emanate with appropriate spin and coning angles through primary nozzles of circular cross sections.

The hubless rotary–jet design was originally conceived as one that might significantly improve performance. However, the single model tested did not provide thrust augmentations comparable to previous rotary–jet designs, largely because of the difficulty of making rational choices for each of the multitude of parameters without the benefit of good computational models and parametric optimization studies. The relatively poor performance could well be because of inappropriate location of the nozzles with respect to the shroud, inappropriate spin and coning angles, and because of the excessive bearing friction inherent in a ball-bearing of such large diameter.

Although the hubless ejector did not achieve the desired levels of performance, it is an excellent configuration for fundamental experimental and computational analysis because of its extremely clean and simple geometry. Such a flowfield is amenable to probing with laser velocimetry, hot-wire anemometry, and for flow visualization. For computational modeling, it is clearly amenable to finite element analysis, because of its relatively clean skew-symmetric geometry.

The goal of this study was to obtain a general fundamental understanding of the complex processes occurring inside the ejector, and to form a basis for determining the validity or invalidity of the hypotheses employed in the theoretical mod-

els. It was therefore decided at the outset that the work would proceed, even though it was clear that the hubless ejector employed in these experiments was far from optimal.

Experiment

Facilities[13]

The experiments were carried out in the George Washington University Propulsion Laboratory using a two-stage rotary blower air supply. All experiments were performed utilizing a hubless rotary–jet similar to that shown in the schematic diagram of Fig. 1c under static conditions in the open laboratory. The test rig was suitably equipped to measure thrust, plenum stagnation conditions, rotor speed, and primary mass flow rate. Measurements were made utilizing hot-wire anemometry, single-component laser anemometry, pitot tubes, and flow visualization using a helium bubble generator, smoke, tufts, and oil films.

Setup and Procedure

The hubless rotary–jet was designed to allow the rotor to be changed. Two rotors were tested in this series of experiments. They were nearly identical except for the spin angles as indicated in Table 1. As a control on the experiments, a rotor was fabricated with zero spin-angle so that the primary jets emerged in the plane of the axis. This ejector was a steady-flow ejector with identical geometry to the rotary–jet, with the sole exception of the nozzle orientation. Clearly, in the ejector with the zero spin-angle rotor, flow induction takes place by turbulent entrainment with the work of interface pressure forces absent.

As seen in Fig. 1c, the hubless rotary–jet consists of an entrance section, a constant area section into which is embedded the rotor with primary nozzles, and a diffuser section. The geometrical parameters of the rotary–jet test rig are given in Table 1.

The ejector was run at a constant pressure ratio of 1.48 for all tests on both the ejector with the rotating primary and the geometrically similar ejector with the nonrotating primary. The flow was subsonic throughout. The resulting test conditions and performance metrics are shown in Table 1. Note that the mass flow rate for the rotating configuration was higher than that for the nonrotating configuration because of the lower static pressures at the exits of the nozzles.

After the test flow conditions were allowed to reach the steady state, as shown in Table 1, the flowfield was mapped throughout the internal region of the ejector using various measuring probes mounted on a traversing system to enable measurements in polar $(r-\theta-z)$ coordinates. The variables mapped included airspeed as determined from a hot-wire anemometer, tangential and radial velocity components of the secondary as measured by a laser-Doppler velocimeter seeded in the secondary, and static and stagnation pressure as measured with a pitot tube. Fourteen nonequally spaced axial stations (closer spacing being employed near the nozzle exit planes) were used over the 30.5 cm length of the ejector. Radial increments of 5.0 mm, ranging from the axis of the ejector to approximately 5.0 mm from the surface if the ejector were taken. Accounting for vibration, the axial and radial positioning accuracy was within ±1.0 mm. Angular increments of 5 deg were taken, with a repeatability of within 2 deg. During the course of measurements, the traversing mechanism was adjusted to a predetermined axial station, and then incremented in the radial direction. For hot-wire anemometry, the rotation of the rotor was encoded using an optical pickup and data taken at 5-deg increments. For the nonrotating, zero spin-angle, control configuration, the rotor was turned to the appropriate angular increments via an auxiliary low-speed electric motor. For the laser anemometry and pitot tube measurements, at given axial and radial positions, measurements were averaged over 360 deg without angular encoding.

One major source of experimental error is because these measurements were taken over a period of several months and each variable had to be mapped noncontemporaneously. Hence, the data presented are a composite of many measurements taken over a long period of time, rather than simultaneous measurements at an instant of time. However, every effort was made to keep the experimental conditions constant to enable repeatability of the results. Repeatability was checked frequently and the results presented do constitute a reasonable approximation to the fluid physics.

Table 1 Parameters of experiment

Variable	Rotating	Nonrotating
Rotor parameters		
β	15 deg	0 deg
α	30 deg	30 deg
Ejector parameters		
Number of nozzles	4	4
Primary nozzle area, A_p, cm^2	2.84	2.84
Ejector throat area, A_s, cm^2	20.3	20.3
Diffuser exit area, A_e, cm^2	7.62	——
Ejector area ratio, A_s/A_p	7.10	——
Diffuser area ratio, A_e/A_s	2.25	——
Diffuser length, cm	14.5	14.5
Overall ejector length, cm	30.5	30.5
Test conditions		
Rotor speed, rpm	12,000	0
Pressure ratio, p_p/p_{atm}	1.48	1.48
Primary mass flow rate, kg/s	0.10	0.10

Results and Discussion

Local Airspeed Mapping

The local airspeed was measured by a hot-wire anemometer. Although the anemometer was not sensitive to the direction of flow, the predominant component is clearly axial. Transverse isokinetic contours showing the behavior of the rotating case, taken at sequential axial stations, are shown in Fig. 2a. A representative longitudinal contour of this same data is shown in Fig. 2b, where the longitudinal slice is arbitrarily taken at a meridional angle of 15 deg from the horizontal as seen in Fig. 2a. Correspondence between the transverse stations and corresponding axial positions in the two views is indicated. A similar presentation is made for the nonrotating case in Fig. 2.

The results show that the fluid velocities of the rotating case are higher than in the nonrotating case. The plenum pressures for both configurations were maintained at the same value. However, the rotary–jet ejector, as a consequence of the improved performance, has a lower pressure at the primary nozzle discharge. This gives rise to a higher primary velocity at the exit of the nozzles.

The results suggest that the rotation has a stabilizing effect so that the rotating jets maintain their integrity over a larger axial distance than the stationary jets of the nonrotating case. Another effect of importance is that the rotating jets tend to hug the wall, whereas the nonrotating jet configuration tends to rapidly move towards the axis of the ejector. While one is anxious to attribute this to the effect of centrifugal forces, trajectories of the fluid particles do not necessarily follow the jets in a nonsteady flow such as this. For the rotating case, the high-velocity regions become nearly parallel to the axis of the ejector very soon after emerging from the nozzles. This supports the assumption of Foa[2] and Hohenemser[7] that the deflection phase is very short. The relative uniformity of the speed over a long axial distance suggests that the assumption of negligible entrainment during the deflection phase has validity. The stability of the jets over a long axial distance is not nec-

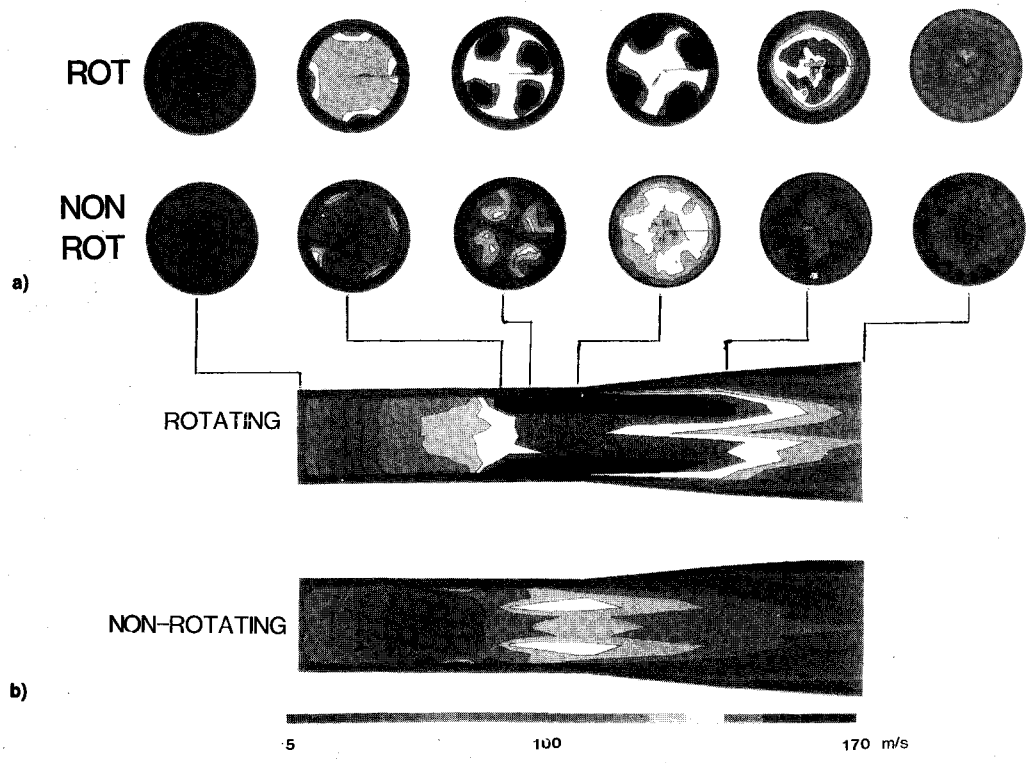

Fig. 2 Local speed contours.

essarily a beneficial attribute if one is to obtain maximum flow induction, since mixing is desirable after the relatively short pressure exchange zone to expedite energy transfer from primary to secondary, and to ensure efficient diffuser performance.

It is expected that the kinematics of the fluid particles in the rotating configuration would be heavily influenced by bearing friction, which is zero in the ideal case, but substantial in this experiment. It is likely that a major improvement in performance could be achieved by substantially reducing bearing friction.

Of interest is the uniformity of the flow at the exit of the diffuser. Comparing the patterns in Fig. 2 at the exit plane, it is clear that the rotating case manifests greater uniformity and that the rotating case is less susceptible to boundary-layer separation. This was corroborated with flow visualization studies in the diffuser. The contention that the optimal rotary jet ejector can be considerably shorter than its nonrotating counterpart is also supported.

Tangential and Radial Velocity Components of Secondary Flow

The laser Doppler velocimeter (LDV), in the backscatter mode, was used to make measurements of the tangential and radial velocity components. The system was not capable of sensing the sign of the velocity component. Hence, there is ambiguity as to whether the flow is radially inward or outward, or tangentially clockwise or counterclockwise. Flow reversals could not be detected. The geometry of the system did not permit the axial velocity component to be measured with the LDV. As a result of the limited focal length of the optics, measurements were taken from the entrance of the ejector to an axial position just downstream of the nozzles. Because of the beam angle and the ejector geometry, measurements were not possible within 5 mm of the walls. Seeding was provided to the secondary only, hence, LDV measurements apply only to the secondary flow. Although it was originally our intention to seed the primary as well, time did not permit resolving the difficulties encountered. Furthermore, our laser velocimeter was not equipped with rotary encoding, and so measurements were averaged over a rotation. It is likely that because of the nonuniformity of the flow, the nonsteady nature of the flow, and preferential particle migration, a substantial bias exists so that at a given radial and axial probe position, the average particle velocity measured with the LDV, averaged over thousands of rotations, may not be a numerically accurate measure of the average secondary fluid velocity.

Despite the aforementioned limitations on the use of the LDV, the ability of the system to isolate the radial and tangential components of velocity was of great value. Since the dominant velocity component in calculating speed is the axial velocity component, and while the hot-wire measurements provide a reasonable approximation to the axial velocity component, the LDV permits study of the much smaller in magnitude, but phenomenologically very important, radial and tangential components.

Figure 3a shows a contour plot of the time-averaged secondary flow tangential velocity component for the rotating nozzle ejectors. For the nonrotating case, which is not shown, one would expect from symmetry that the only mechanism for introducing a tangential component is the inherent turbulence in the flow. The LDV measurements indicated that the turbulence level was relatively low in the nonrotating case as no perceptible tangential component could be measured. For this reason, the contour plot for these measurements is not shown. For the rotating case, however, Fig. 3a clearly suggests that a vortex core forms near the axis. When Fig. 3a is compared with Fig. 2b, it is suggested that the primary jets tend to stay closer to the wall while driving a rotational core flow near the axis. The fact that the tangential component does not approach zero on the axis of rotation can be attributed to the imperfect axial symmetry of the apparatus, probe vibration, and the turbulence level. It is expected that the magnitude of this tangential velocity component would decrease as the rotor bearing friction is eliminated, the behavior of the rotor more closely approximating the ideal free-spinning condition. In the case of the free-spinning rotor, conservation of angular momentum requires that the secondary flow tangential velocity component be in corotation with the rotor, while the primary is in counterrotation. Since bearing friction was not negligible in this test,

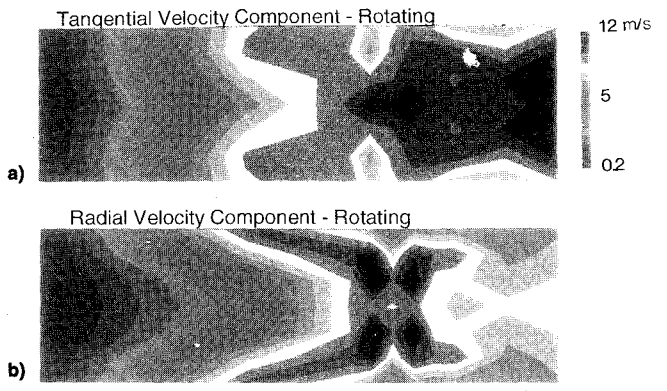

Fig. 3 Meridional mean velocity components in tangential and radial directions.

the angular momentum of the primary was enhanced by bearing torque, which was then imparted to the secondary.

In Fig. 3b the meridionally averaged radial component of secondary velocity for the rotational case is shown. This figure may be understood by noting that as the primary rotates and the secondary fluid is deflected to accommodate the traversing primary, the local radial secondary velocity component may be positive or negative, depending on the angular position. The data shown in Fig. 3b are an average, whose sign is undetermined. Hence, interpretation of Fig. 3b is difficult. However, it may be observed that near the nozzles the region of maximum radial velocity is in the proximity of the jets. The magnitude of the radial component is comparable to that of the tangential component. This is an indication of the poor design of the present ejector in that rather than exchange momentum with the primary, the secondary circumvents the primary and avoids the interaction. Different ejector geometries should ameliorate this deficiency. The fact that it is nonzero on the axis again reflects the reasoning previously applied in the tangential case.

Time Mean Stagnation Pressure

A pitot tube probe was traversed throughout the ejectors to measure stagnation pressure distributions in both nonrotating and rotating ejectors and averaged over 360 deg of angular position at each radial and axial position of the probe. In an ideal ejector without energy dissipation, one would expect to see a sudden increase in average stagnation pressure at the exit plane of the nozzles as the energetic primary performs work on the secondary. Afterwards, any change in the meridional average stagnation pressure indicates dissipation of energy. The actual results are shown in Figs. 4a and 4b for the nonrotating and rotating ejectors, respectively.

In the nonrotating case, it can be seen that after emanation from the nozzles, the mean stagnation pressure rapidly decreases near the nozzle exit plane. However, after this interaction, the radial profile of stagnation pressure becomes fairly uniform. This is consistent with the previous observation that intense mixing occurs. The axial diminution of the magnitude of the meridional average stagnation pressure is suggestive of substantial dissipation of energy in the interaction zone. Another negative characteristic of the nonrotating ejector is the obviously strong tendency for separation in the diffuser.

For the rotating case, the situation appears quite different. The exchange between primary and secondary of energy appears to be very nondissipative and effective at the periphery. The highly elongated shape of the contours suggests a nondissipative process and a reasonable approximation to the ideal. However, at the core of the ejector, the exchange of energy from the primary to the secondary is very ineffective. This may provide an indication of why this hubless configuration has hitherto failed to provide the levels of thrust augmentation achieved by previous hubbed versions. A large part

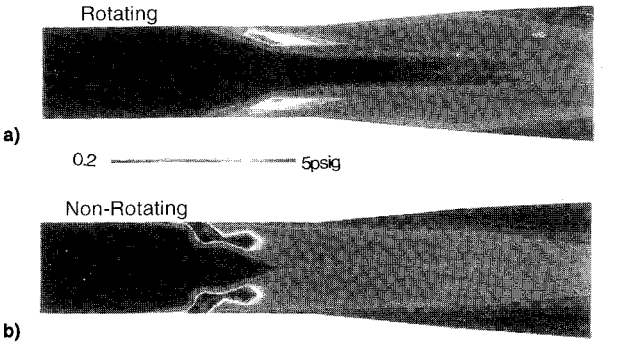

Fig. 4 Meridional mean stagnation pressure.

of the flow passed through the core without effective flow induction. However, the results do demonstrate less dissipative flow induction mechanism of the rotary–jet ejector which, with proper design, could lead to improved performance. Separation in the diffuser of the rotating ejector is clearly seen in Fig. 4a. However, rotation ameliorates the problem in comparison with the nonrotating case. Thus, the rotary jet enables a shorter ejector design not only by virtue of the nonsteady flow induction mechanism, but also by virtue of its tendency to stabilize the diffuser.

Conclusions

Theoretical predictions on the performance of rotary–jet thrust augmenters have consistently indicated a high potential benefit for the utilization of nonsteady flow effects. However, while experimental results have been superior to comparable steady-flow ejectors, expectations have not yet been realized. This study has provided, for the first time, some insight into the complex flow phenomena that occur inside the ejector. Notwithstanding the clear suggestion that the underlying assumptions of the models were reasonable for an optimal ejector, the study shows clearly why the experimental design leaves much room for improvement.

The results show that the work of nonsteady flow interface pressure forces occurs over a very short axial distance and, consistent with previous models, entrainment during this process is negligible. This offers the possibility of a very short ejector. The results show that applying the work of nonsteady pressure forces uniformly across the secondary is a problem and the results suggest that a design which confines the initial primary/secondary interaction to an annular zone is preferable. The results demonstrate the adverse effects of bearing friction that produce an undesirable core vortex. Separation in the diffuser is seen to be a problem alleviated by the rotary–jet design. The results show that stagnation pressure loss in the rotary–jet design is reduced, suggesting a higher energy transfer efficiency.

Achievement of an optimal design has been hampered by the complexity of the flowfield, the large number of geometrical parameters, and the high cost of fabricating sophisticated test models. This study has illuminated some of the important characteristics of the flowfield and should facilitate the next generation of rotary–jet ejector designs.

Acknowledgments

This work was supported by Grant NAG-3-860 from NASA Lewis Research Center. This support is gratefully acknowledged. We would also like to express our appreciation to Colin Drummond for his enthusiastic interest in the project and his many insightful and stimulating discussions.

References

[1]Lockwood, R. M., and Patterson, W. G., "Energy Transfer from an Intermittent Jet to a Secondary Fluid in an Ejector-Type Thrust Augmenter," Hiller Aircraft Co. Rept. ARD-305, Palo Alto, CA, June 1962.

[2]Foa, J. V., "A New Method of Energy Exchange Between Flows and Some of Its Applications," Rensselaer Polytechnic Inst. TR AE5509, Troy, NY, Dec. 1955.

[3]Foa, J. V., "Direct Flow Induction," George Washington Univ., TR-82-FI1, Washington, DC, March 1982.

[4]Hohenemser, K. H., and Porter, J. L., "Contribution to the Theory of Rotary-Jet Flow Induction," *Journal of Aircraft*, Vol. 3, No. 4, 1966, pp. 339–346.

[5]Costopoulos, T., "Constant-Area Flow Interaction in Crypto Steady Flow Thrust Augmenters," George Washington Univ., TR-UTA-773, Washington, DC, April 1977.

[6]Foa, J. V., and Garris, C. A., "Cryptosteady Modes of Direct Fluid-Fluid Energy Exchange," *Machinery for Direct Fluid-Fluid Energy Exchange*, AD-07, American Society of Mechanical Engineers, New York, 1984.

[7]Hohenemser, K., "Flow Induction by Rotary Jets," *Journal of Aircraft*, Vol. 3, No. 1, 1966, pp. 18–24.

[8]Hohenemser, K., and McBrayer, J. D., "Effect of Density Ratio on Rotary Jet Flow Induction," *Journal of Aircraft*, Vol. 8, No. 4, 1969, pp. 208–212.

[9]Sladky, J. F., "Experimental Tests on a Crypto-Steady Augmenter," Final Rept., Contract N00161-79-C-0013, U.S. Naval Academy, Annapolis, MD, Nov. 1980.

[10]Porter, J. L., "Hot Gas Rotary Jet Flow Induction," McDonald Douglas Corp. Rept. F744, St. Louis, MO, Aug. 1967.

[11]Cordier, S., "Rotary-Jet Thrust Augmenter with Jet-Flapped Blades," Ph.D. Dissertation, George Washington Univ., Washington, DC, Aug. 1989.

[12]Garris, C. A., Toh, K. H., and Xie, L., "A New Concept for a Hubless Rotary Jet," AIAA/SAE/ASME/ASEE 27th Joint Propulsion Conf. (Sacramento, CA), AIAA, Washington, DC, June 1991.

[13]Amin, S., "Non-Steady Flow Induction: An Experimental Investigation," Ph.D. Dissertation, George Washington Univ., Washington, DC, Dec. 1994.